

# Make a Donut: Hierarchical EMD-Space Planning for Zero-Shot Deformable Manipulation with Tools

Yang You<sup>1,✉</sup>, Bokui Shen<sup>1</sup>, Congyue Deng<sup>1</sup>, Haoran Geng<sup>2</sup>, Songlin Wei<sup>2</sup>, He Wang<sup>2</sup>, Leonidas Guibas<sup>1,✉</sup>

**Abstract**—Deformable object manipulation stands as one of the most captivating yet formidable challenges in robotics. While previous techniques have predominantly relied on learning latent dynamics through demonstrations, typically represented as either particles or images, there exists a pertinent limitation: acquiring suitable demonstrations, especially for long-horizon tasks, can be elusive. Moreover, basing learning entirely on demonstrations can hamper the model’s ability to generalize beyond the demonstrated tasks. In this work, we introduce a demonstration-free hierarchical planning approach capable of tackling intricate long-horizon deformable manipulation tasks without necessitating any training. We employ large language models (LLMs) to articulate a high-level, stage-by-stage plan corresponding to a specified task. For every individual stage, the LLM provides both the tool’s name and the Python code to craft intermediate subgoal point clouds. With the tool and subgoal for a particular stage at our disposal, we present a granular closed-loop model predictive control strategy. This leverages Differentiable Physics with Point-to-Point correspondence (DiffPhysics-P2P) loss in the earth mover distance (EMD) space, applied iteratively. Experimental findings affirm that our technique surpasses multiple benchmarks in dough manipulation, spanning both short and long horizons. Remarkably, our model demonstrates robust generalization capabilities to novel and previously unencountered complex tasks without any preliminary demonstrations. We further substantiate our approach with experimental trials on real-world robotic platforms. Our project page: <https://qq456cvb.github.io/projects/donut>.

## I. INTRODUCTION

Manipulation of deformable objects remains one of the most intricate challenges in robotics due to the inherent complexity and unpredictable behavior of such objects. Deformable objects can be broadly categorized into two major categories: thin-shell surfaces, such as clothes [1], [2] and ropes [3]; and volumetric objects, such as dough [4], [5]. In this paper, we focus on the latter and study dough manipulation given a set of candidate tools like rolling pin, knife, etc.

Existing works on dough-like volumetric deformable objects majorly rely on a learned dynamic model of the underlying particles [6], [7], [8]. However, these methods

all require a substantial amount of collected or semi-auto-generated demonstrations for training the dynamic models, which poses two critical issues: firstly, the difficulty of obtaining a comprehensive set of demonstrations, particularly for long-horizon tasks; and more importantly, the limited capability of generalizing beyond the scope of the provided demonstrations.

Given this context, there is an imperative need for a more versatile and universally applicable approach to deformable object manipulation, one that can navigate the intricacies of both short and long-horizon tasks, without being overly reliant on demonstrations. This paper introduces a novel demonstration-free hierarchical planning method that addresses these challenges.

In this study, we delve into the manipulation of dough, a quintessential example of deformable object manipulation [4], [9], [5] with tools. As illustrated in Figure 1, our approach takes a natural language user prompt as input and leverages a large language model (LLM) to formulate a high-level plan detailing the selection of tools and the representation of intermediate subgoals at each phase. While LLMs might not produce precise low-level actions for each timestep, they exhibit proficiency in breaking down intricate tasks into manageable stages. Each of these stages exclusively involves a single tool and a piece of dough.

The concept of anchoring language to a sequential plan has been investigated in prior research [10], [11], [12]. However, such methodologies have largely been confined to generating high-level linguistic instructions for robots for generic household tasks (e.g., “open the fridge” or “bring me the apple”). They haven’t been tailored for intricate tasks like deformable object manipulation. Indeed, there is a significant gap in literature when it comes to utilizing LLMs for manipulating deformable entities, especially when the challenge entails crafting complex shapes (like donuts or baguettes) based purely on linguistic outputs. In our approach, rather than defining the robot’s actions or policy linguistically at intermediate stages, we direct LLMs to express their object-centric state visualizations via Python code. This distinctive approach sets our method apart from previous techniques.

In bridging adjacent subgoal imaginations generated from LLMs, we introduce a simple but novel EMD space planning algorithm complemented by model predictive control. The algorithm evaluates the gradient of the earth mover’s distance between the prevailing point cloud and the target point cloud concerning each discrete point. Subtracting this gradient from the current point cloud yields the succeeding viable

<sup>1</sup>Yang You, Bokui Shen, Congyue Deng, Leonidas Guibas are with Department of Computer Science, Stanford University, the US.

<sup>2</sup>Haoran Geng, Songlin Wei, He Wang are with CFCS, Peking University, China.

Contact email: {yangyou, guibas}@stanford.edu

The research is supported in part by the Toyota Research Institute University 2.0 Program and a Vannevar Bush Faculty Fellowship. Yang You is also supported in part by the Outstanding Doctoral Graduates Development Scholarship of Shanghai Jiao Tong University.

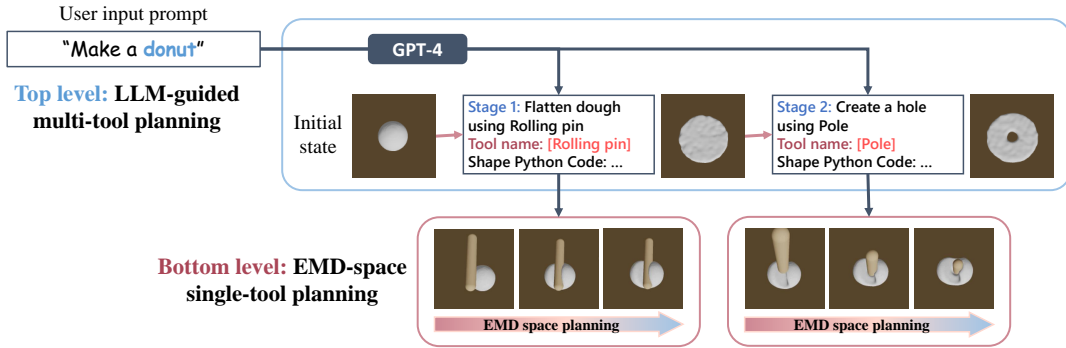


Fig. 1: **Schematic illustration of our method in handling unseen dough making tasks**, where Language Models (LLMs) are utilized at a high level for task decomposition and subgoal generation, specifying tool names and generating corresponding Python code. The low-level operates on particle space controls, precisely determining the next achievable candidate iteratively without the need for prior demonstrations or task-specific training.

candidate. This process facilitates a direct point-to-point correspondence between the existing state and the upcoming candidate, enabling the deployment of differentiable physics based on a straightforward per-point mean squared error.

Through this hierarchical strategy, our system can adeptly tackle novel, intricate tasks devoid of any demonstrations or prior training, given a set of candidate tools. Experimental results demonstrate that our methodology markedly enhances the efficacy of both single-tool and multiple-tool dough manipulation with various tools and can potentially transfer to real-world robotic applications.

## II. RELATED WORKS

*a) Differentiable physics for deformable object manipulation:* Differentiable physics is a pivotal technique in deformable object manipulation. It exploits the gradient from differentiable simulators to derive optimal actions. Existing literature [13], [14], [15] reveals that differentiable physics offers an efficient means to tackle short-horizon simple tasks. Nevertheless, as highlighted by [16], the reliance of differentiable physics on local gradients poses challenges. The loss landscape is often rugged with potentially spurious local optima, making it less reliable for certain tasks.

*b) Long-horizon planning for deformable object manipulation:* There’s an emerging interest in long-horizon strategies for deformable object manipulation. DiffSkill [9] employs a latent space planner to assess various skill combinations and sequences to achieve the desired outcome. Subsequently, PASTA [4] introduced the PPlanning with Spatial-Temporal Abstraction framework, melding spatial and temporal abstraction for effective long-horizon task planning. Robocraft [17] advances a particle-based dynamics model using graph neural networks (GNNs) to grasp the system’s structural nuances. This knowledge is then harnessed to optimize action sequences from a randomly initialized trajectory. Robocook [18] adopts point cloud scene representation and leverages GNNs for modeling tool-object interactions. It then synergizes tool classification with self-supervised policy learning for crafting object manipulation plans. Nonetheless, these methodologies have their constraints. They necessitate

prior insight into potential tool candidates and a predetermined number of stages, which affects their adaptability.

*c) Language models for robot manipulations:* Leveraging large language models for robotics is currently a bustling research domain. Recent studies such as [10], [12], [11] strive to dissect complex tasks into manageable sub-stages. These methods, although innovative, are primarily innocent to the underlying geometry, providing only high-level robot directives. To enrich these models with diverse modalities, SM [19] developed a modular framework where new tasks are delineated as a linguistic interaction between pre-trained models and auxiliary modules, underpinned by Socratic reasoning. PaLM-E [20] engineered a versatile embodied multimodal language model tailored for a spectrum of downstream reasoning challenges. VoxPoser [21] harnesses LLMs to craft voxel value maps in a 3D observation space, guiding robot-environment interactions. Since LLMs often cannot directly produce the robot’s raw actions, an alternative approach is to map intricate tasks to rewards. Some other studies [22], [23] focus on curating domain-specific reward models, which necessitate abundant annotated training data. In contrast, works like [24] generate reward metrics automatically from pretrained LLMs, though their application is predominantly limited to rigid or articulated objects. Deformable object manipulations remain a relatively under-explored territory for LLMs, largely due to the immense degrees of freedom inherent to such tasks and the paucity of available demonstration data.

## III. METHOD

Given a set of candidate common tools to accomplish a complex dough manipulation task, our method adopts a hierarchical planning approach combining both language models and low-level particle space controls. At the top level, LLMs are employed to break down a complex task into sub-stages, and output both the code to generate subgoal states and the tool name for each. We observe that LLMs obtain rich knowledge about high-level task semantics though cannot directly output raw low-level actions. At the bottom level, given the current tool and subgoal, our technique iteratively identifies the next reachable target based on the present state

and subgoal. A key distinction between our approach and previous ones is that ours doesn’t necessitate any demonstration or training for the target task. In Section III-A, we detail the partitioning of complex tasks into sub-stages and the associated tools. Section III-B elaborates on the iterative process of determining the next goal based on the current state and subgoal.

An overview of our method is illustrated in Figure 1. Our method processes the sampled particles from the volumetric dough as input and produces the actions of the currently used tool as output. In the subsequent context, we will interchangeably use point clouds and particles.

### A. Multiple Tool Selection and Hierarchical Planning

To address the challenge of coordinating between different tools in long-horizon tasks, we turn to the capabilities of large language models (LLMs), especially ChatGPT-4 [25]. Our observations indicate that while LLMs may not precisely produce low-level actions, they excel in deconstructing intricate long-horizon tasks into several stages, each centered around a single tool. What’s more, for each of these stages, the LLM can both identify the appropriate tool and generate the corresponding Python code to produce intermediate subgoal point clouds. Presented in the form of particles, these subgoals readily align with the target requirements of our proposed single-tool EMD space planning algorithm.

To guide this process, we devised a prompt template that imparts to the LLM foundational information about available tools and their potential interactions with the dough. Additionally, we introduce a set of guidelines designed to refine and direct the LLM when completing more complex, long-horizon deformable tasks. One important guideline is to force the LLM to give volume-preserving input and output at each stage, so the target is more physically realistic. In addition, we leverage the chain reasoning technique [26] to help the LLM better deduce the shape parameters to satisfy this constraint. In Table I, we provide the average relative volume change between the LLM’s generated final output and the input dough for all the three evaluated tasks. Details of the prompt template can be found on our project website.

	Donut ↓	Baguette ↓	TwoPancakes↓
w/o VP and CR	73.9%	42.5%	65.0%
Ours	<b>9.8%</b>	<b>38.9%</b>	<b>0.0%</b>

TABLE I: **Volume change with and without volume-preserving (VP) and chain reasoning (CR).**

In addition, we also ask the LLM to output the following items for each stage during planning:

- A one-line explanation of what this step is doing.
- The name of the tool to be used.
- The Python code to generate target point clouds. Do remember to add their absolute world location when generating complex shapes.
- The variable names for the input and output.

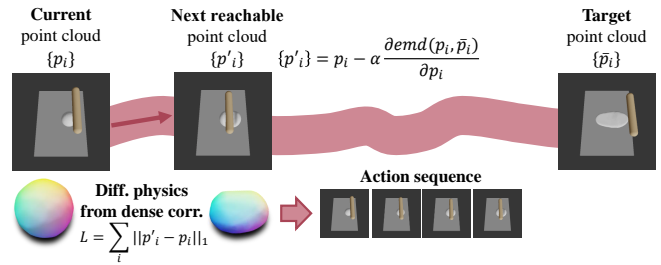


Fig. 2: **EMD-space planning with DiffPhysics-P2P.** We find the next reachable target by running small steps within the EMD space. The induced point-to-point correspondence can provide better gradients when optimizing actions through differential physics.

- The location of each piece in a dictionary format with a variable name as the key.
- The volume of each piece is also in a dictionary format with a variable name as the key.

Building on this, we only extract the generated Python code corresponding to each stage, from which we produce the intermediate subgoal point cloud. Other outputs, though not used, are part of chain reasoning and, therefore contribute to the final quality of the generated subgoal. The subgoal point cloud is then fed directly into our single-tool planning module. Consequently, we are equipped to tackle intricate tasks incrementally, stage by stage, eliminating the need for demonstrations.

### B. Single Tool Planning

As the LLM can decompose a complex task into several stages with generated sub-targets, on each stage, given the current point cloud and the sub-target, we introduce a novel closed loop planning algorithm.

Our method initially identifies an optimal starting position for the tool. Subsequently, it forecasts the nearest attainable target and refines the actions employing differentiable physics with point-to-point correspondences, termed DiffPhysics-P2P. If this step doesn’t yield progress, our model reverts the actions and re-strategizes using a new starting position. This process repeats for several steps until we reach the target goal or hits the maximum number of steps. The algorithm is summarized in Algorithm 1.

a) *DiffPhysics-P2P*: Given the current observation and the goal, we pinpoint the subsequent reachable point cloud by executing multiple small iterations (specifically 20 in our experiments) of gradient descent within the Earth Mover Distance (EMD) space. Formally, each iteration is:

$$\mathbf{p}'_i = \mathbf{p}_i - \alpha \cdot \frac{\partial \text{demd}(\{\mathbf{p}_i\}, \{\bar{\mathbf{p}}_i\})}{\partial \mathbf{p}_i}. \quad (1)$$

In other words, given the current point cloud observation, denoted as  $\mathbf{p}_i$ , where  $i$  is the point index, and the subgoal  $\bar{\mathbf{p}}_i$ , our objective is to discern the ensuing reachable candidate. This is achieved by incrementally transitioning the current point cloud towards the target within the EMD space. The candidate serves as our model’s prediction of the underlying particle dynamics.

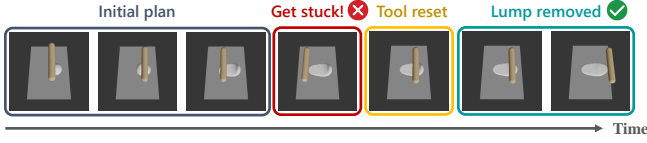


Fig. 3: **Illustration on how tool reset works.** By resetting the tool position when no improvement can be made, we can jump out of the local minima and get a better global solution.

A notable advantage of the EMD gradient is its inherent capacity to furnish a one-to-one correspondence between  $\mathbf{p}'_i$  and  $\mathbf{p}_i$ , as elucidated by Equation 1. This characteristic permits the application of the subsequent straightforward mean-absolute-error loss:

$$L = \sum_i \|\mathbf{p}'_i - \mathbf{p}_i\|_1. \quad (2)$$

This is different from several preceding methodologies, wherein the naive EMD loss (expressed as  $\text{emd}(\mathbf{p}_i, \mathbf{p}'_i)$ ) is employed devoid of any point-to-point correspondence. Ablation studies underscore that our point-to-point correspondence substantially outperforms traditional differential physics by enhancing the gradient flow. An illustration of this algorithm is given in Figure 2.

*b) Initial position selection:* The aforementioned EMD planning algorithm demonstrates efficacy when the initial tool position is in proximity to the dough. However, challenges arise when the tool is situated at a considerable distance from the dough, resulting in the algorithm’s inability to find the global minima. To figure out a good initial position for the tool, we leverage the strategy initially proposed in [27]. Specifically, with the present deformation field deduced from the induced point-to-point correspondence (represented as  $\mathbf{p}'_i - \mathbf{p}_i$ ), we employ the following equation to identify the candidate tool position:

$$\mathbf{x}^* = \arg \max_{\mathbf{x}} \sum_i \frac{\|\mathbf{p}'_i - \mathbf{p}_i\|_1}{\text{sdf}_{\mathbf{x}}(\mathbf{p}_i) + \delta}. \quad (3)$$

The numerator encapsulates the point-to-point correspondence loss of the extant point cloud. In contrast, the denominator represents the signed distance field (SDF) of the tool (plus a small delta  $\delta$ ) when positioned at  $\mathbf{x}$ , evaluated at particle  $\mathbf{p}_i$ , representing distance from the tool to the dough.

*c) Tool reset upon failures:* Integrating the previously described techniques allows us to first select an optimal initial tool position, followed by iteratively progressing towards the target as per Equation 1. However, even with an advantageous starting tool position, challenges may arise due to the inherent intricacies of differentiable physics. As illustrated in Figure 3, consider a scenario where the task is to use a rolling pin to flatten the dough into a sphere. While initiating from a favorable position, iterating and optimizing candidates in the EMD space could land us at a local minimum. This could result in an uneven texture on one side of the dough, manifesting as a lump. To circumvent this predicament, we reset the tool’s position if no advancement is observed, ensuring an escape from potential local minima.

The comprehensive single-tool closed loop planning process is detailed in Algorithm 1.

---

**Algorithm 1** Closed Loop Planning with Model Predictive Control

---

**Input:** Current system particles  $\{\mathbf{p}_i\}$ , target particles  $\{\tilde{\mathbf{p}}_i\}$   
**Output:** Predicted actions at each timestep  $\{\mathbf{a}_t\}$

- 1:  $t := 0, need\_reset := 1, \text{emd}_{last} := \infty$
- 2: **while**  $t < max\_steps$  **do**
- 3:    $\{\mathbf{p}'_i\} := \{\mathbf{p}_i\}$
- 4:   **for**  $k$  **in**  $1 \dots K$  **do**
- 5:      $\{\mathbf{p}'_i\} := \{\mathbf{p}'_i\} - \alpha \cdot \nabla_{\{\mathbf{p}'_i\}} \text{emd}(\{\mathbf{p}'_i\}, \{\tilde{\mathbf{p}}_i\})$  ▷
- 6:     Move particles along the gradient within emd space
- 7:   **end for**
- 8:   Set  $\{\mathbf{p}'_i\}$  as the next reachable candidate
- 9:   **if**  $need\_reset$  **then**
- 10:      $\mathbf{x}^* = \arg \max_{\mathbf{x}} \frac{\|\mathbf{p}'_i - \mathbf{p}_i\|_1}{\text{sdf}_{\mathbf{x}}(\mathbf{p}_i) + \delta}$  ▷ Find the optimal initial tool position
- 11:     Set initial tool position to  $\mathbf{x}^*$
- 12:      $need\_reset = 0$
- 13:   **end if**
- 14:    $\mathbf{a}_{t:t+L} := \mathbf{0}$  ▷ Initialize actions for horizon  $L$
- 15:   **for**  $j$  **in**  $1 \dots J$  **do**
- 16:      $\mathbf{a}_{t:t+L} := \mathbf{a}_{t:t+L} - \nabla_{\mathbf{a}} \text{Sim}(\sum_i \|\mathbf{p}'_i - \mathbf{p}_i\|_1)$  ▷ Differential physics with point-to-point correspondence
- 17:   **end for**
- 18:   Execute  $\mathbf{a}_{t:t+L}$  and get the new particle observation  $\{\tilde{\mathbf{p}}_i\}$  ▷  $\{\tilde{\mathbf{p}}_i\}$  may differ from  $\{\mathbf{p}'_i\}$
- 19:    $\text{emd}_{curr} := \text{emd}(\{\tilde{\mathbf{p}}_i\}, \{\tilde{\mathbf{p}}_i\})$  ▷ Calculate the actual emd after executing  $\mathbf{a}_{t:t+L}$
- 20:   **if**  $\text{emd}_{curr} > \text{emd}_{last}$  **then** ▷ No progress
- 21:      $need\_reset = 1$  ▷ Find another initial position to escape local minimum
- 22:   **continue**
- 23:   **end if**
- 24:   **if**  $\text{emd}_{curr} < \tau$  **then**
- 25:     **break**
- 26:   **end if**
- 27:    $t = t + L, \text{emd}_{last} = \text{emd}_{curr}, \{\mathbf{p}_i\} = \{\tilde{\mathbf{p}}_i\}$
- 28: **end while**

---

### C. Implementation Details on Simulated Experiments

Our simulation environments are in line with established dough manipulation literature, notably Lin et al. [9], [4]. We employ both DiffTaichi [13] and PlastineLab [5] to handle differentiable physics. Following the common practice, we combine three distinct losses with coefficient (1, 1, 0.02) when optimizing actions with differentiable physics:

- 1) The point-to-point loss described in Section IV-B.
- 2) An SDF loss that make the tool close to the dough.
- 3) A velocity regularization loss.

We use a parameter  $max\_steps = 200$ ,  $K = 20$  and  $L = 40$ . We make use of the Adam optimizer with a learning rate set at 0.02 during the differentiable physics computations. For the emd loss computation, our approach leans on the GeomLoss [28] library available in Pytorch. When searching

for the optimal tool position, we consider the tightest axis-aligned bounding box plus a small offset above the dough depending on each tool’s shape.

#### IV. EXPERIMENT

In our experiments, we validate the efficacy of our method across four distinct dimensions. In Section IV-A, we deploy our hierarchical LLM-guided planning algorithm to more intricate and unseen long-horizon tasks. In Section IV-B, we conduct simpler tasks involving only one tool to authenticate the effectiveness of our single-tool planning algorithm. In Section IV-C, we perform distinct ablation studies for both single-tool and multiple-tool planning algorithms. In Section IV-D, we translate our simulated actions to a real-world robot to manipulate the actual dough, illustrating the practical applicability of our method from sim to real.

*a) Baselines:* We employ the following baselines for comparisons: Firstly, we consider a simplistic gradient-based action optimization method utilizing differentiable physics, denoted as Diff. Physics. Secondly, we examine a sophisticated long-horizon planning algorithm, PASTA [4], which integrates both spatial and temporal abstraction. Thirdly, we explore a behavior cloning method that trains a goal-conditioned policy, abbreviated as BC. Lastly, we assess a model-free RL method, SAC-N [29]. For complex tasks, generating a large dataset of demonstrations is intractable. Thus we manually annotate a single demonstration sequence for each task for training BC and SAC-N. For PASTA, we employ its pre-trained model on single-tool demonstrations and assess its generalization capabilities on these unseen, intricate tasks. All the compared methods receive the point cloud of particles as input.

*b) Metrics:* We adopt the metrics in [9], [4] and report the normalized decrease (score) in the Earth Mover Distance (EMD), which is computed using the Sinkhorn divergence as  $\frac{\text{emd}(\{\mathbf{p}_0\}, \{\mathbf{p}^*\}) - \text{emd}(\{\mathbf{p}_T\}, \{\mathbf{p}^*\})}{\text{emd}(\{\mathbf{p}_0\}, \{\mathbf{p}^*\})}$ , where  $\{\mathbf{p}_0\}$  is the initial point cloud,  $\{\mathbf{p}_T\}$  is the final point cloud after execution, and  $\{\mathbf{p}^*\}$  is the ground-truth target 3D point cloud. Additionally, we also calculate the success rates based on pre-set thresholds (Appendix A).

For each multiple-tool task, we utilize the LLM’s Python code output from the last stage to generate the point cloud, serving as the ground truth. We observe that these point clouds, despite being generated by the LLM, are of high quality and adeptly describe the target shape. For single-tool tasks, we follow previous literature [4], [9] to sample 5 random targets at different shapes and locations. Samples of the generated target point clouds are shown in Appendix C. For each multiple-tool task, we generate 4 distinct responses from the LLM, with each response being assessed 5 times, culminating in a total of 20 trials per task; for each single-tool task, we follow previous literature to evaluate one trial per target, resulting in 5 trials per task.

##### A. Multiple-Tool Selection and Planning

*a) Environment setup:* We examine three intricate long-horizon tasks that necessitate the use of multiple tools:

Donut, Baguette, and TwoPancakes. As implied by their names, these tasks require the agent to create a donut, a baguette, and two pancakes, respectively. In the TwoPancakes task, the dough is initially presented as a rectangle. For the Donut and Baguette tasks, the dough is initially provided in the form of a unit ball. A more comprehensive description of each task can be found in Appendix A.

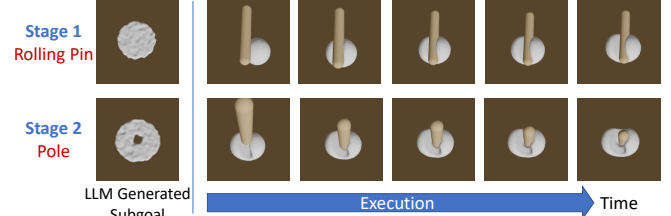


Fig. 4: “**Make a Donut.**” An exemplary zero-shot execution on complex long-horizon tasks.

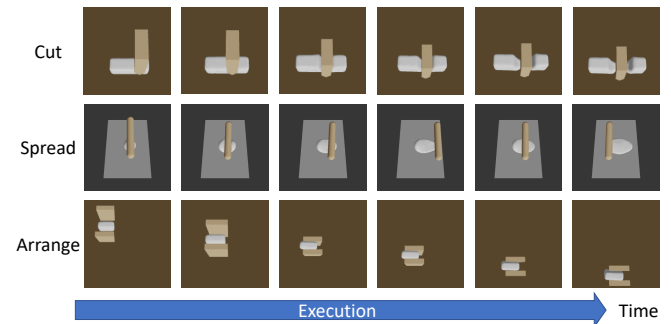


Fig. 5: **Cut, spread, arrange.** Single-tool execution results.

*b) Results:* The quantitative results are presented in Table II’s left. It is evident from the data that our method substantially surpasses preceding approaches, exhibiting superior performance across all three tasks by a considerable margin. It is crucial to underscore that our model has never been exposed to these tasks before, and it employs the high-level stage plans generated by the LLM and the single-tool EMD space planning method to dynamically generate actions. A detailed, stage-by-stage visual representation of the process is provided in Figure 4, illustrating the nuanced steps and strategies employed by our method in navigating and accomplishing the tasks. More qualitative results are given in Appendix D.

The key distinction of our approach lies in its zero-shot learning ability, which enables it to adapt to novel tasks without task-specific fine-tuning or training. This is a significant leap over the sampled-based methods, which may not provide a feasible path or require extensive data for complex shapes. The Large Language Model (LLM) plays a crucial role in our framework by charting a high-level planning path, which serves as a guide for the subsequent execution by the low-level Earth Mover’s Distance (EMD) space planning algorithm. This hierarchical structure is pivotal; the LLM alone cannot translate its generated plans into the raw actions required for robotic manipulation. Conversely, without the strategic direction provided by the LLM, the EMD space planning lacks a coherent objective, struggling to discern

what end states are physically plausible for the robot to achieve. PASTA, while effective within its demonstrated scope, requires a dataset to train on in order to sample feasible intermediate states and is thus inherently limited in its ability to generalize to new shapes, e.g., donut. All their modules like VAE, cost predictor, etc., are tailored to their collected training data. This data-driven dependency hinders its application to the more complex tasks our framework successfully tackles.

Method	Multiple-tool tasks			Single-tool tasks		
	Donut	Baguette	TwoPancakes	Spread	Cut	Arrange
Diff. Physics [14]	0.141/0%	0.175/20%	0.583/0%	0.184/20%	0.401/60%	0.296/20%
PASTA [4]	0.020/0%	-0.116/0%	-0.856/0%	0.155/20%	0.060/40%	0.052/0%
BC	0.001/0%	-0.606/0%	0.220/0%	0.441/60%	-0.488/20%	-0.512/0%
SAC-N [29]	0.003/0%	-0.306/0%	0.127/0%	0.000/0%	-2.827/0%	0.267/0%
Ours	<b>0.346/75%</b>	<b>0.501/75%</b>	<b>0.858/65%</b>	<b>0.680/100%</b>	<b>0.685/100%</b>	<b>0.981/100%</b>

TABLE II: Quantitative comparisons on both single-tool and multiple-tool tasks.

### B. Single-Tool Planning

a) *Environment setup*: In the simulation environment provided by PASTA [4], we examine three elementary tasks related to dough manipulation: Spread, Cut, and Arrange. Each of these tasks necessitates the use of only one tool at a time and can be finished within 200 time steps. More task descriptions can be found in Appendix A.

b) *Results*: Quantitative outcomes are presented in Table II’s right. It is evident that our approach consistently surpasses previous baselines by a substantial margin. The baselines fail to accomplish these tasks, whereas our method attains a 100% success rate in all of them. It is also noteworthy that, in contrast to prior learning-based approaches, our method does not necessitate any demonstration data. Remarkably, our method does not even entail any training, rendering it immediately applicable to new tasks. Qualitative results are illustrated in Figure 5.

### C. Ablation Studies

a) *Multiple-tool ablations*: Figure 6 presents our ablation studies on planning without the incorporation of high-level plans generated by the LLM. Additionally, we conduct ablation on the volume-preserving guidance with chain reasoning, which is proved to be crucial for maintaining both a high success rate and consistent target volume generation.

b) *Single-tool ablations*: Figure 7 presents our ablation studies on the removal of the DiffPhysics-P2P, the initial position selection component, or the tool resetting module within the single-tool planning algorithm.

### D. Real-Robot Experiments

a) *Environment setup*: The application of this algorithm to a real-world robot is of immense interest. For this purpose, an experimental setup is established using the UFACTORY xArm 6 and some clay. Given the experimental setting and observations, the proposed planning algorithm is used to generate a trajectory in the simulator, and subsequently, the controller is employed to execute this trajectory in the real world. Unlike that in simulation, we do not have the ground-truth volumetric particle state in real-world experiments.

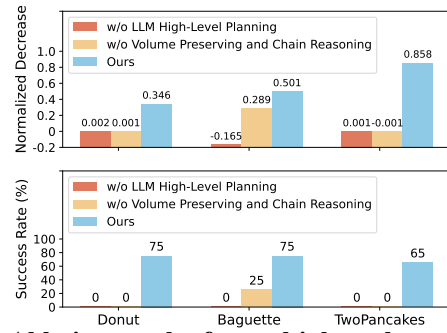


Fig. 6: Ablation results for multiple-tool experiments.

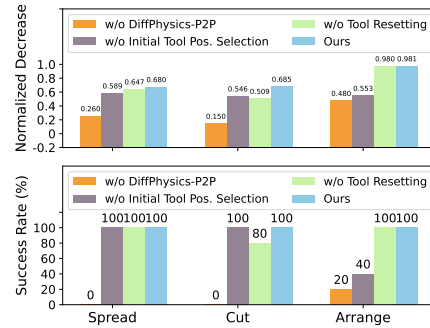


Fig. 7: Ablation results for single-tool experiments.

In order to estimate the particle from observations, we setup four cameras from the four orthogonal directions and utilize truncated signed distance function (TSDF) fusion [30] to reconstruct volumetric particles from multi-view depth cameras. In Figure 8, qualitative real-robot trajectories are provided for making a donut. A real-world manipulation demo video is given in the supplementary.

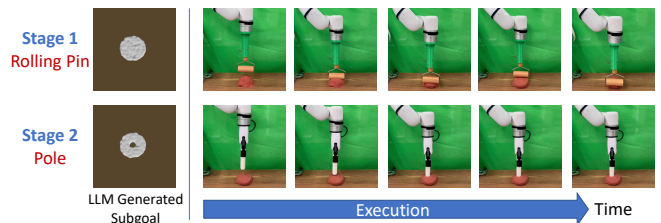


Fig. 8: “Make a donut.” The robot first flattens the dough and uses the pole to create a hole.

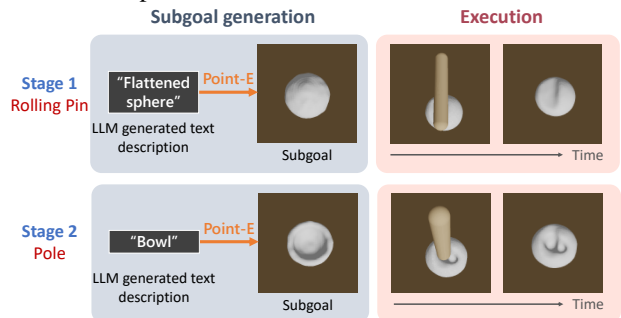


Fig. 9: “Make a bowl.” An example that leverages off-the-shelf text-to-3D algorithms to generate complex shapes.

## V. CONCLUSIONS AND LIMITATIONS

We introduced a new hierarchical planning method for robotic deformable object manipulation, enabling complex tasks without prior demonstrations. This method surpasses

previous demonstration-based techniques, ensuring better adaptability to new scenarios. Using large language models, it generates high-level plans and intermediate goals, which are executed through a unique closed-loop predictive control using Differentiable Physics. Our approach showed exceptional performance and adaptability in dough manipulation benchmarks, marking a significant step forward in deformable object manipulation.

*a) Limitations:* While our method is adept at handling complex tasks involving long-horizon planning, it is limited to generating simple shapes that can be described with the Python codes produced by the LLM. Generating Python code to describe the shape of an arbitrary object is extremely challenging, if not impossible, for nowadays’ LLM. However, we have made efforts to circumvent this limitation by having the LLM generate intermediate text descriptions that can be input into state-of-the-art Text-to-3D generative models, such as Point-E [31]. Figure 9 illustrates an example of creating a bowl from the dough. The shape of a bowl is difficult to describe using pure Python code, so the LLM outputs text descriptions for each subgoal, like “Flattened Sphere” and “Bowl”. These text are then interpreted by Point-E to generate point clouds. We then proceed with our planning, using these point clouds as intermediate targets.

Besides, the dimensions and morphology of candidate tools are pre-determined as a priori constraints, consequently limiting the range of tasks that can be undertaken. A compelling avenue for future research could be to investigate the simultaneous optimization of the size of these tools, or let the LLM be aware/decide the size of the tools.

## APPENDIX

### A. Detailed Descriptions for each task

#### a) Single-Tool Tasks:

- **Spread:** Spread is a task where the dough is initially a ball. The target is to use a rolling pin to flatten it into a flat sphere. The threshold for this task is 0.4.
- **Cut:** Cut is a task where the dough is initially an elongated box. The target is to cut the dough into two pieces in the middle with a knife. The threshold is 0.4.
- **Arrange:** Arrange is a task where the dough is initially a box. The target is to move the dough using a gripper to another place. The threshold is 0.7.

#### b) Multiple-Tool Tasks:

- **Donut:** Donut is a task where the dough is initially a ball. The target is to create a donut-shaped dough. The threshold for this task is 0.3.
- **Baguette:** Baguette is a task where the dough is initially a ball. The target is to create a baguette-shaped dough. The threshold for this task is 0.5.
- **TwoPancakes:** TwoPancakes is a task where the dough is initially an elongated box. The target is to make two pancake-shaped doughs. The threshold is 0.85.

### B. Hyperparameters for Simulation Dough

We use PlasticineLab [5] to simulate the dough. PlasticineLab is a Python environment that is suitable for de-

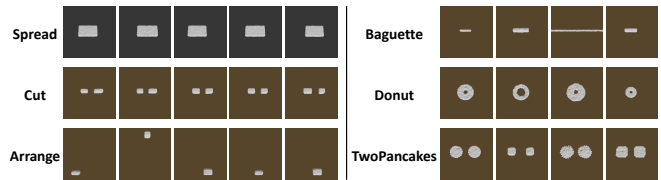


Fig. 10: **LLM-generated target point clouds. Left:** Single-tool tasks. **Right:** Multi-tool tasks.

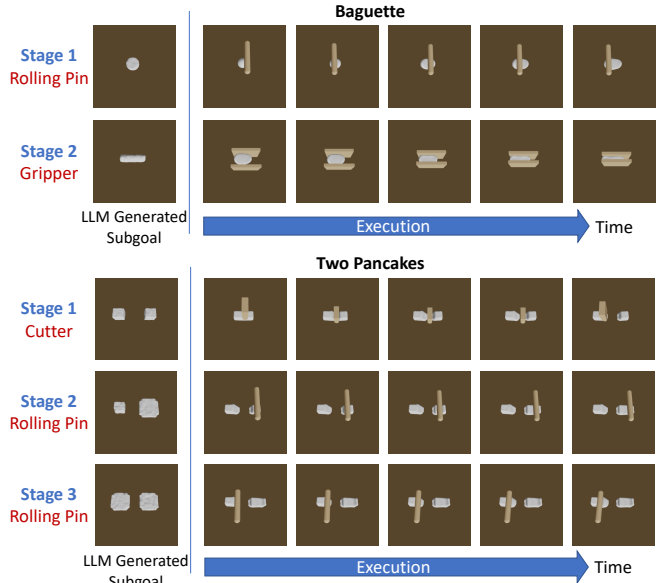


Fig. 11: Execution trajectory of our method with intermediate subgoals set by the LLM.

formable object simulation. The hyperparameters that are relevant to the properties of the dough are identical to those in PASTA [4] to ensure a fair comparison.

### C. Target Point Clouds Visualization

*a) Single-tool tasks:* For single-tool tasks, we follow PASTA [4] to generate 5 random target dough point clouds at different places or shapes, as shown in Figure 10 left.

*b) Multiple-tool tasks:* For multiple-tool tasks, we utilize the LLM’s Python code output from the last stage to generate the point cloud, serving as the ground truth. We observe that these point clouds, despite being generated by the LLM, are of high quality and adeptly describe the target shape. Visualizations are illustrated in Figure 10 right.

### D. Intermediate Subgoal Visualization

Figure 11 depicts more execution trajectories of our method, including intermediate goals generated by the Language Learning Model (LLM). While LLM may not produce subgoals that are perfectly reachable for execution, the closed-loop execution with EMD space point-to-point planning (DiffPhysics-P2P) algorithm within our approach exhibits resilience to such imperfections.

### E. Next Reachable Point Cloud Visualization

In this section, we visualize the topological change of next reachable point clouds throughout the process of making a

donut. The visualizations demonstrate key stages, such as the intentional alteration of the dough’s topology to create a hole in the middle of a donut. In this context, the intrinsic property of optimal transport (OT) that does not necessarily preserve topological structures is leveraged to our advantage. Although our tools may not execute the point cloud to perfection, the LLM-generated subgoals guide the gradient flow towards the target. The methodology allows for self-correction with each observation, ensuring that each step brings us closer to the intended outcome.

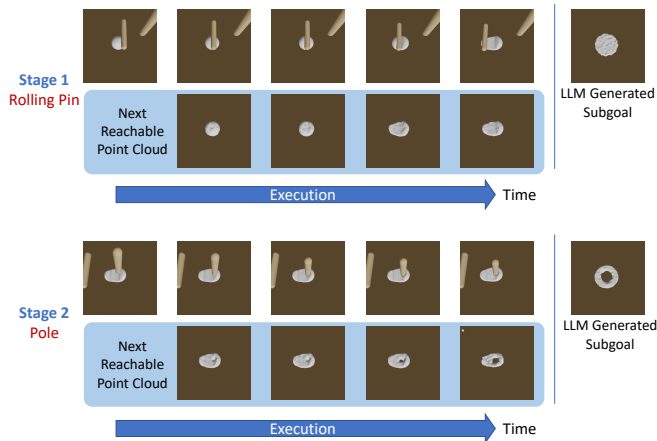


Fig. 12: Next reachable point cloud visualization for making a donut. Notice that the topology is gradually changed during the second stage for making the donut. The LLM planning phase ensures that subsequent OT steps are guided towards physically realizable subgoals.

## REFERENCES

- [1] O. Nocentini, J. Kim, Z. M. Bashir, and F. Cavallo, “Learning-based control approaches for service robots on cloth manipulation and dressing assistance: a comprehensive review,” *Journal of NeuroEngineering and Rehabilitation*, vol. 19, no. 1, pp. 1–25, 2022.
- [2] Y. Wu, W. Yan, T. Kurutach, L. Pinto, and P. Abbeel, “Learning to manipulate deformable objects without demonstrations,” *arXiv preprint arXiv:1910.13439*, 2019.
- [3] P. Sundaresan, J. Grannen, B. Thananjeyan, A. Balakrishna, M. Laskey, K. Stone, J. E. Gonzalez, and K. Goldberg, “Learning rope manipulation policies using dense object descriptors trained on synthetic depth data,” in *2020 IEEE International Conference on Robotics and Automation (ICRA)*. IEEE, 2020, pp. 9411–9418.
- [4] X. Lin, C. Qi, Y. Zhang, Z. Huang, K. Fragkiadaki, Y. Li, C. Gan, and D. Held, “Planning with spatial-temporal abstraction from point clouds for deformable object manipulation,” in *Conference on Robot Learning (CoRL)*, 2022.
- [5] Z. Huang, Y. Hu, T. Du, S. Zhou, H. Su, J. B. Tenenbaum, and C. Gan, “Plasticinelab: A soft-body manipulation benchmark with differentiable physics,” *arXiv preprint arXiv:2104.03311*, 2021.
- [6] J. Zhu, A. Cherubini, C. Dune, D. Navarro-Alarcon, F. Alambeigi, D. Berenson, F. Ficuciello, K. Harada, J. Kober, X. Li, *et al.*, “Challenges and outlook in robotic manipulation of deformable objects,” *IEEE Robotics & Automation Magazine*, vol. 29, no. 3, pp. 67–77, 2022.
- [7] V. E. Arriola-Rios, P. Guler, F. Ficuciello, D. Kragic, B. Siciliano, and J. L. Wyatt, “Modeling of deformable objects for robotic manipulation: A tutorial and review,” *Frontiers in Robotics and AI*, vol. 7, p. 82, 2020.
- [8] H. Yin, A. Varava, and D. Kragic, “Modeling, learning, perception, and control methods for deformable object manipulation,” *Science Robotics*, vol. 6, no. 54, p. eabd8803, 2021.
- [9] X. Lin, Z. Huang, Y. Li, J. B. Tenenbaum, D. Held, and C. Gan, “Diffskill: Skill abstraction from differentiable physics for deformable object manipulations with tools,” *arXiv preprint arXiv:2203.17275*, 2022.
- [10] W. Huang, P. Abbeel, D. Pathak, and I. Mordatch, “Language models as zero-shot planners: Extracting actionable knowledge for embodied agents,” in *International Conference on Machine Learning*. PMLR, 2022, pp. 9118–9147.
- [11] M. Ahn, A. Brohan, N. Brown, Y. Chebotar, O. Cortes, B. David, C. Finn, C. Fu, K. Gopalakrishnan, K. Hausman, *et al.*, “Do as i can, not as i say: Grounding language in robotic affordances,” *arXiv preprint arXiv:2204.01691*, 2022.
- [12] J. Liang, W. Huang, F. Xia, P. Xu, K. Hausman, B. Ichter, P. Florence, and A. Zeng, “Code as policies: Language model programs for embodied control,” in *2023 IEEE International Conference on Robotics and Automation (ICRA)*. IEEE, 2023, pp. 9493–9500.
- [13] Y. Hu, L. Anderson, T.-M. Li, Q. Sun, N. Carr, J. Ragan-Kelley, and F. Durand, “DiffTaichi: Differentiable programming for physical simulation,” *arXiv preprint arXiv:1910.00935*, 2019.
- [14] Y. Hu, J. Liu, A. Spielberg, J. B. Tenenbaum, W. T. Freeman, J. Wu, D. Rus, and W. Matusik, “Chainquean: A real-time differentiable physical simulator for soft robotics,” in *2019 International conference on robotics and automation (ICRA)*. IEEE, 2019, pp. 6265–6271.
- [15] J. Liang, M. Lin, and V. Koltun, “Differentiable cloth simulation for inverse problems,” *Advances in Neural Information Processing Systems*, vol. 32, 2019.
- [16] R. Antonova, J. Yang, K. M. Jatavallabhula, and J. Bohg, “Rethinking optimization with differentiable simulation from a global perspective,” in *Conference on Robot Learning*. PMLR, 2023, pp. 276–286.
- [17] H. Shi, H. Xu, Z. Huang, Y. Li, and J. Wu, “Robocraft: Learning to see, simulate, and shape elasto-plastic objects with graph networks,” *arXiv preprint arXiv:2205.02909*, 2022.
- [18] H. Shi, H. Xu, S. Clarke, Y. Li, and J. Wu, “Robocook: Long-horizon elasto-plastic object manipulation with diverse tools,” *arXiv preprint arXiv:2306.14447*, 2023.
- [19] A. Zeng, M. Attarian, B. Ichter, K. Choromanski, A. Wong, S. Welker, F. Tombari, A. Purohit, M. Ryoo, V. Sindhwani, *et al.*, “Socratic models: Composing zero-shot multimodal reasoning with language,” *arXiv preprint arXiv:2204.00598*, 2022.
- [20] D. Driess, F. Xia, M. S. Sajjadi, C. Lynch, A. Chowdhery, B. Ichter, A. Wahid, J. Tompson, Q. Vuong, T. Yu, *et al.*, “Palm-e: An embodied multimodal language model,” *arXiv preprint arXiv:2303.03378*, 2023.
- [21] W. Huang, C. Wang, R. Zhang, Y. Li, J. Wu, and L. Fei-Fei, “Voxposer: Composable 3d value maps for robotic manipulation with language models,” *arXiv preprint arXiv:2307.05973*, 2023.
- [22] P. Goyal, S. Niekum, and R. J. Mooney, “Using natural language for reward shaping in reinforcement learning,” *arXiv preprint arXiv:1903.02020*, 2019.
- [23] J. Lin, D. Fried, D. Klein, and A. Dragan, “Inferring rewards from language in context,” *arXiv preprint arXiv:2204.02515*, 2022.
- [24] M. Kwon, S. M. Xie, K. Bullard, and D. Sadigh, “Reward design with language models,” *arXiv preprint arXiv:2303.00001*, 2023.
- [25] OpenAI, “Gpt-4 technical report,” 2023.
- [26] J. Wei, X. Wang, D. Schuurmans, M. Bosma, F. Xia, E. Chi, Q. V. Le, D. Zhou, *et al.*, “Chain-of-thought prompting elicits reasoning in large language models,” *Advances in Neural Information Processing Systems*, vol. 35, pp. 24 824–24 837, 2022.
- [27] S. Li, Z. Huang, T. Du, H. Su, J. B. Tenenbaum, and C. Gan, “Contact points discovery for soft-body manipulations with differentiable physics,” *arXiv preprint arXiv:2205.02835*, 2022.
- [28] J. Feydy, T. Séjourné, F.-X. Vialard, S.-i. Amari, A. Trounev, and G. Peyré, “Interpolating between optimal transport and mmd using sinkhorn divergences,” in *The 22nd International Conference on Artificial Intelligence and Statistics*, 2019, pp. 2681–2690.
- [29] G. An, S. Moon, J.-H. Kim, and H. O. Song, “Uncertainty-based offline reinforcement learning with diversified q-ensemble,” *Advances in neural information processing systems*, vol. 34, pp. 7436–7447, 2021.
- [30] A. Zeng, S. Song, M. Nießner, M. Fisher, J. Xiao, and T. Funkhouser, “3dmatch: Learning local geometric descriptors from rgb-d reconstructions,” in *CVPR*, 2017.
- [31] A. Nichol, H. Jun, P. Dhariwal, P. Mishkin, and M. Chen, “Point-e: A system for generating 3d point clouds from complex prompts,” *arXiv preprint arXiv:2212.08751*, 2022.